energies

MDPI

Article

An Auxiliary Passive Circuit and Control Design for Wireless Power Transfer Systems in DC Microgrids with Zero Voltage Switching and Accurate Output Regulations

Hu Xiong [1], Bin Xiang [1] and Yuan Mao [2,*]

[1] Electric Power Research Institute, State Grid Hubei Electric Power Co., Ltd., Wuhan 430077, China
[2] College of Information Engineering, The Zhejiang University of Technology, Hangzhou 310023, China
* Correspondence: maoyuan@zjut.edu.cn; Tel.: +86-0571-85290616

Abstract: This paper presents an auxiliary passive circuit and control design for wireless power transfer (WPT) systems in DC microgrids to achieve optimal power transfer efficiency while maintain accurate output voltage regulation. An auxiliary inductance is added at the transmitter resonator to form a current sink to ensure zero voltage switching (ZVS) of the primary-side full-bridge inverter with even extremely light load conditions. Moreover, an adaptive proportional–integral (PI) controller is adopted to track the output voltage references by regulating the phase shift angle of the phase shift control for the full-bridge inverter. The coefficients of the adaptive PI controller are determined by the inductance of the auxiliary inductance. Both simulation and experimental results validated the effectiveness of the proposed circuit and control design in achieving optimal efficiency and output voltage regulation for WPT systems in DC microgrids with source and load variations.

Keywords: wireless power transfer (WPT); DC microgrids; optimal efficiency; zero voltage switching (ZVS); output voltage regulation

Citation: Xiong, H.; Xiang, B.; Mao, Y. An Auxiliary Passive Circuit and Control Design for Wireless Power Transfer Systems in DC Microgrids with Zero Voltage Switching and Accurate Output Regulations. *Energies* **2023**, *16*, 694. https://doi.org/10.3390/en16020694

Academic Editor: Alicia Triviño-Cabrera

Received: 1 December 2022
Revised: 28 December 2022
Accepted: 3 January 2023
Published: 6 January 2023

1. Introduction

With the emergence of energy crisis and environmental pollution problems, electric vehicles (EVs) are regarded as one of the essential methods to alleviate environmental concerns. The rapid growth of EVs has pushed the higher requirement for more reliable charging methods. Wireless power transfer (WPT), as one of the promising alternatives of traditional wired charging, can address the issues of easily broken power cables and electric shocks under the harsh environments of EVs [1,2]. DC microgrids, due to their higher efficiencies, easier integration into electric devices, and simpler control over their AC counterparts, have gained increasing attention in recent years [3–8]. Future WPT-based EV charging infrastructures have great potential to be integrated into DC microgrids. An imaginary diagram of WPT-based EV charging in DC microgrids is shown in Figure 1. When WPT is adopted in high-power applications, large amplitudes of primary-side voltages and currents can lead to significant power loss on the driving circuits. Therefore, it is crucial to design coils, circuits, and controls of WPT systems to achieve optimal efficiencies while still maintaining accurate output regulations.

A typical WPT system for EV charging in DC microgrids comprises (i) a full-bridge inverter at the front end to convert DC voltage to high-frequency AC voltage, (ii) a coupled resonator with compensated circuits at both transmitter and receiver sides, (iii) a diode bridge rectifier and a filter capacitance, and (iv) a battery load, which can be modelled as pure resistance [9–11]. The efficiency of the WPT system is mainly determined by the conduction loss on the equivalent series resistances (ESRs) of the resonators and switching loss on the full-bridge inverters. Thereinto, the conduction loss on the ESRs can be reduced by using high-quality resonator coils, while the switching loss on the inverters can be minimized by achieving zero voltage switching (ZVS).

Figure 1. An imaginary diagram of WPT-based EV charging in DC microgrids.

There are four switches in the primary side of the circuit of the WPT system, and all of them have parasitic capacitance and internal resistance. When the switch tube is turned on, its voltage cannot instantly drop to 0, and its current cannot immediately rise to a stable value. Both voltage and current changes take a certain amount of time, and there will be an overlap between the voltage and current, resulting in conduction losses. The same happens when the switch is turned off. They are called hard-switching problems. Under the same circuit settings, the switch always produces the same loss in each switching period, and the loss is proportional to the switching frequency. The switching loss caused by hard switching limits the increase in the frequency of the inverter, thereby also limiting the miniaturization and weight reduction of the inverter. To reduce the size and weight of the inverter, it is necessary to increase the frequency [12]. Therefore, soft-switching technology was born to solve the conduction loss problem caused by high frequency.

In WPT systems, a transformer or a coupled coil can transfer energy from the primary side to the secondary side of the circuit through the magnetic field. The coils are compensated with different circuits to achieve the maximum transfer efficiency at the resonant frequency. There are four compensation circuits in the WPT system that are most common, namely: series–series (S-S), series–parallel (S-P), parallel–parallel (P-P), and parallel–series (P-S) [13,14]. Soft-switching technology mainly uses the capacitance and inductance in the circuit to adjust the topology in order to avoid current and voltage overlapping as much as possible.

The development of soft-switching technology since the 1970s is shown in Table 1 [15].

Table 1. Development history of soft-switching technology.

Time	Name	Application
1970s	Series resonant converters, SRCs and series parallel converters, PRCs	Half-bridge or full-bridge converters
Early 1980s	Active clamp technology	Mainly single-ended converters
Mid 1980s	Quasi-resonant converters, QRCs and multi-resonant converters, MRCs	Single-ended or bridge converter
Late 1980s	ZVS PWM and ZCS PWM	Single-ended or bridge converter
Late 1980s	Phase-shifted zero-voltage-switching PWM DC/DC full-bridge converter, PS ZVS FB converter	Full-bridge converter over 250 W

In the early 1970s, soft-switching technology mainly used series or parallel resonance technology. The DC converter is also called a resonant converter. The resonant converter has three modes of operation defined by the switching frequency. f is the working fre-

quency and f_r is the resonant frequency. When $f < 1/2f_r$, the resonator is in the current discontinuous working mode, and the switch tube works under the condition of ZCS. When $1/2f_r < f < f_r$, the resonant tank is capacitive. Therefore, the current leads the voltage when the switch is turned off, and the overlap area becomes smaller. However, the current–voltage overlap area becomes more significant when the switch is turned on as hard switching. When $f_r < f$, the resonant circuit is inductive, and the switch tube is turned on with ZVS, but the hard switching happens when turning off. Series or parallel resonance technology is used in some communication switching power supplies, and the switching frequency ranges from 180 to 450 kHz.

The active clamp ZVS technology proposed later is mainly used in single-ended converters. The authors of [16] proposed an active clamp ZVS PWM converter design for satellite power supply. Such converters can be implemented with single-ended forward and fly back circuits and their combinations. Taking the active clamp single-ended fly back converter as an example, this converter adds a clamping capacitance and a MOSFET as a clamping switch on the basis of the PWM single-ended fly back circuit. The circuit also utilizes the resonance in the circuit. The parasitic capacitance of the MOSFET and the inductance in the transformer or coupling inductance resonate, so that the main switch can be turned on at zero voltage.

Based on S-P resonance technology, quasi-resonant conversion technology and multi-resonance conversion technology became popular in the next decade [17,18]. Initially, it was to realize the soft-switching of the converter composed of a single tube. Still, the push–pull converter, the half-bridge converter, and the full-bridge converter can also participate in the quasi-resonant converter and the multi-resonant converter. The difference between the quasi-resonant converter and the series–parallel resonance technology proposed in the 1970s is that it adds a resonant inductance and a resonant capacitance to the DC converter in the resonant converter. This resonant inductance and resonant capacitance reconstitute a resonant tank. According to the different combinations of series and parallel of inductance and capacitance in the resonant tank, the switch tube can realize ZVS or ZCS [19]. The resonant tank of a multi-resonant converter is different from that of a quasi-resonant converter. The resonant tank of the multi-resonant converter is composed of the general resonant tank, the leakage inductance of the transformer, and the parasitic capacitance in the circuit [20]. According to the working principle of the multi-resonant converter and quasi-resonant converter, it can be seen that they also use frequency modulation. This is also a disadvantage because it is challenging to design the output filter for the system using frequency modulation. Therefore, quasi-resonant converters and multi-resonant converters are generally used with low power and low voltage, and with strict requirements on volume and weight.

Since the early resonant circuits all required frequency modulation control, which brought great difficulty to the design of the filter, the converter based on constant frequency control was proposed in the later period. This kind of converter is also called the ZVS PWM converter. The ZVS PWM converter adds an auxiliary switch tube to the quasi-resonant converter in the circuit structure. It controls the resonant tank by controlling the conduction of the auxiliary switch tube. In the ZVS PWM converter, the resonant tank does not always participate in the resonance as before but only works in resonance at the moment when the switch tube is switching [21]. Therefore, the working time of the resonant tank occupies only a small part of the switching period.

Full-bridge converters are generally used in medium and high-power occasions such as electric vehicle charging. In particular, the primary-side phase-shifted (PPS) full-bridge (FB) DC-DC converter is widely used [22–27]. It adopts the phase shift control method, uses the circuit's own parameters to resonate to achieve soft switching, and maintains the PWM technology's characteristics of an adjustable duty cycle based on constant frequency [28].

The main contributions of this paper include

- a new passive auxiliary circuit method for WPT systems in achieving both ZVS and accurate output regulations with conventional phase shift control;

- an investigation of the soft switching for primary-side inverters in WPT systems with a wide range of load conditions;
- a systematic design procedure and parameter selection method for the passive auxiliary circuit.

2. Analysis and Control of Wireless Power Transmission Systems

The main circuit of the wireless charging system used in this paper is shown in Figure 2. The full-bridge inverter consists of a DC source and four MOSFETs which are Q_1 to Q_4. D_1 to D_4 are the intrinsic diodes of Q_1 to Q_4 and C_1 to C_4 are the corresponding capacitances. The resonant tank circuit adopts the S-S compensation circuit. L_p and L_s represent the inductances on the primary and secondary side coils, respectively, and M is the mutual inductance. C_p and C_s are the compensated capacitances. Meanwhile i_p and i_s denote the currents of the primary and secondary circuits, respectively. D_{R1} to D_{R4} represent the four diodes in the full-bridge rectifier. C_f is the filter capacitance and R_{Ld} is the load resistor in the secondary circuit.

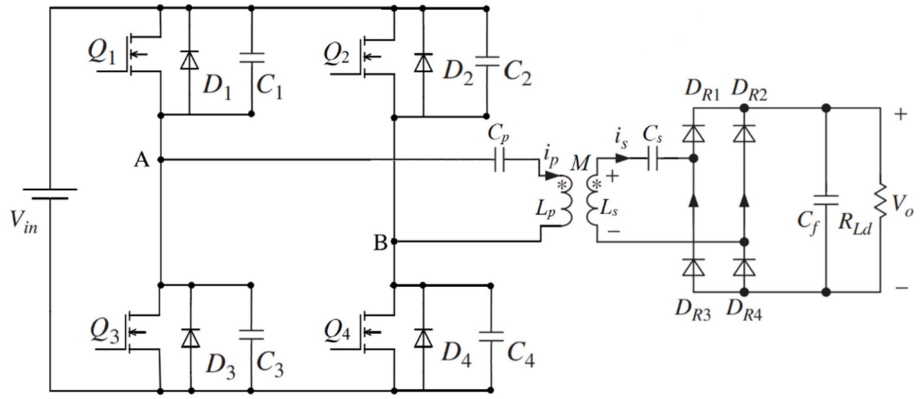

Figure 2. Topology of two-stage WPT system.

The wireless charging system uses the phase-shifted full-bridge control mode. Q_1 and Q_3 are called leading legs, and Q_2 and Q_4 are called lagging legs. Figure 3 shows a possible switching signal waveform for MOSFETs. δ is the phase shift angle. Fully compensated resonance occurs at the same operating frequency on both the primary and secondary side of the circuit.

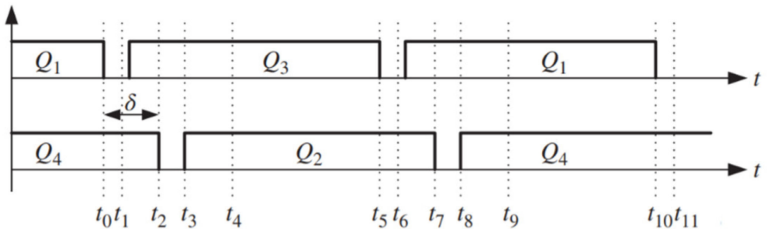

Figure 3. Example signal waveform of MOSFETs.

A stable output voltage is essential for wireless charging systems. Therefore, the system needs a control circuit to realize the closed-loop control of the circuit. The flow chart of the control circuit is shown in Figure 4. The proportional–integral (PI) controller will output a phase angle between the leading and the lagging leg. The control loop then generates two sine waves with the phase difference and converts the sine waves into square waves with the same frequency through the comparator. These square waves are the input conduction signals for MOSFETs. Thus, a wireless charging system loop with controllable output voltage is obtained.

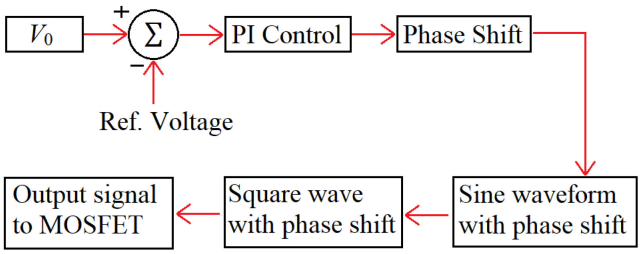

Figure 4. Flowchart of the output voltage closed-loop control.

However, when the system is at the light load condition, the switching tube will have apparent conduction loss due to the large phase shift, which is called hard switching. The following article analyzes in detail the process of hard switching in the WPT system. The different switching modes for the WPT system are shown in Figure 5.

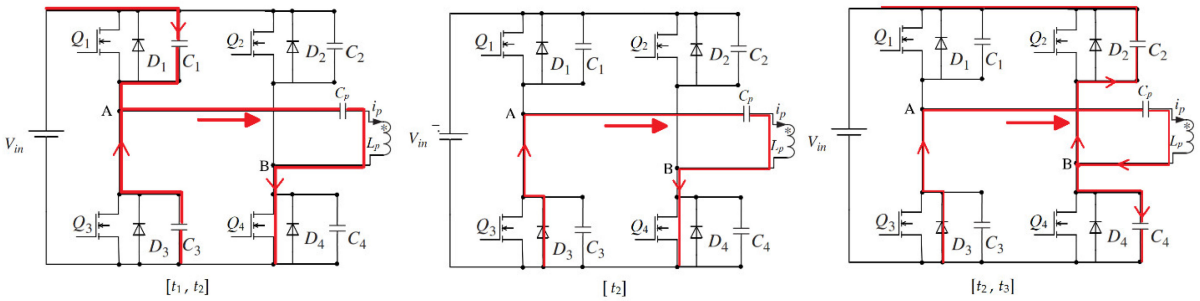

Figure 5. Equivalent circuits of different switching modes in hard-switching condition.

Some assumptions are made before the analysis:

- All switching devices are ideal;
- All capacitances and inductances are ideal regardless of their internal resistance;
- The intrinsic capacitances of the four MOSFETs are all equal in value.

At t_1, Q_1 is turned off. The primary current i_p begins to charge C_1 and discharge C_3. When the voltage of C_1 increases to V_{in} and the voltage of C_3 decreases to 0, this makes D_3 conduct at t_1. Then D_3 clamps the voltage of C_3 at 0. Therefore, Q_3 can achieve ZVS. At t_2, Q_4 is turned off. The primary current i_p still does not reach 0, charging C_4 and discharging C_2. However, when the system is at light load condition, i_p is already very small. Therefore, although i_p can charge and discharge Q_2 and Q_4, it cannot complete the charge and discharge process. As a result, Q_2 and Q_4 cannot achieve ZVS, as shown in Figure 6. At t_3, Q_2 is turned on. i_p flows from B to A in reverse.

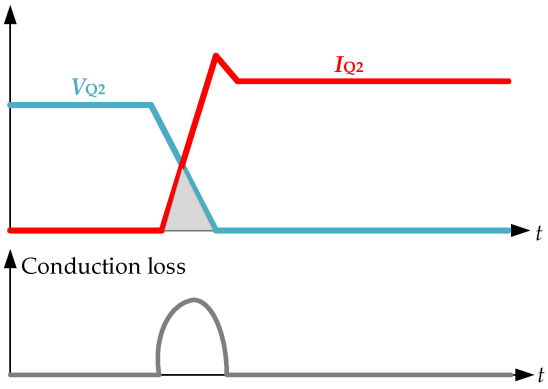

Figure 6. The current–voltage relationship diagram of Q_2 when hard switching occurs [17].

According to the above analysis, it can be concluded that under the light load condition, the phase shift of the feedback system output is very large. Hence the lagging leg cannot

achieve ZVS and results in a significant loss, while the leading leg does not have such a hard-switching problem. Therefore, although the system can realize the controllable output voltage, it needs to solve the conduction loss problem of the lagging leg.

3. Solutions and Analysis to Improve Hard Switching in WPT Systems

In Section 2, i_p drops to 0 before charging and discharging of the lagging leg is completed. If i_p is large enough to finish the charging and discharging, Q_2 can achieve ZVS. Hence it is considered to place a current source at point B, as shown in Figure 7a. The current source is used to increase the charging current for the lagging leg to complete the charging and discharging process, and it is typically modelled with a large inductance. The circuit topology after replacing the current source with an inductance is shown in Figure 7b and L_a is the auxiliary inductance.

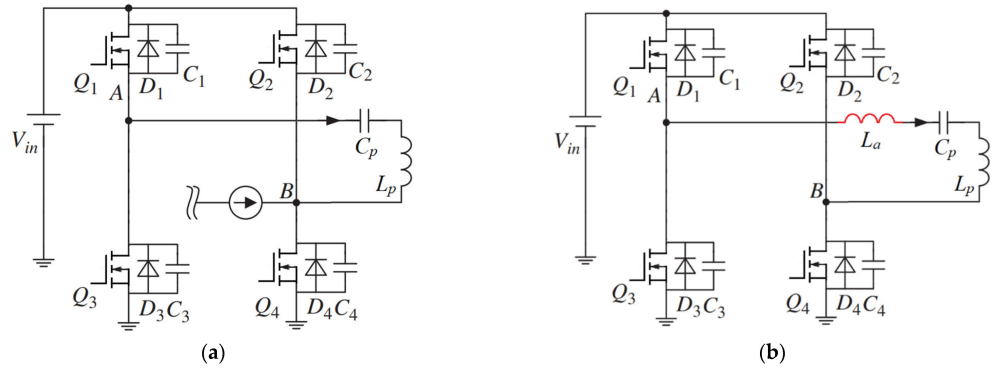

Figure 7. Proposed soft-switching circuit. (**a**) is the topology after adding the current source; (**b**) is the topology after replacing the current source with an inductance.

The control circuit in the WPT system has not changed. The control circuit still feeds back the load voltage mentioned in Section 2 and controls the output voltage by adjusting the phase shift. The auxiliary inductance in the full-bridge inverter is only to solve the hard-switching problem. The following article analyzes the working process of the improved circuit. After adding the auxiliary inductance, the signal for the MOSFETs and the waveform of current and voltage between points A and B are shown in Figure 8.

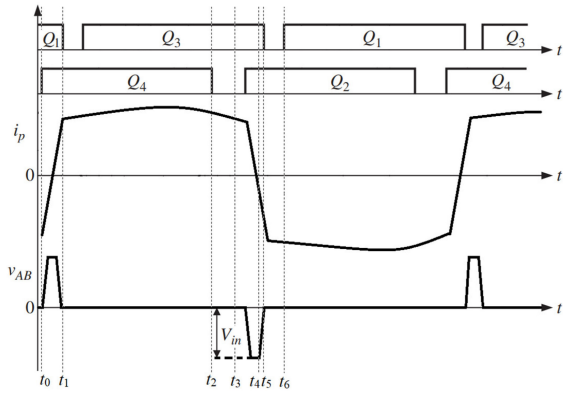

Figure 8. Waveforms of MOSFETs control signals V_{AB}, and i_p for the proposed soft-switching circuit.

In order to better analyze this circuit, the following assumptions are made:

- All switching devices are ideal;
- All capacitances and inductances are ideal regardless of their internal resistance;
- The intrinsic capacitances of the MOSFETs are all equal in value.

The current flow diagram at different time periods is shown in Figure 9.

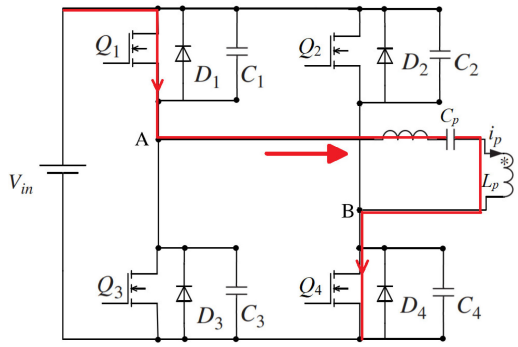

(a) $[t_0, t_1]$

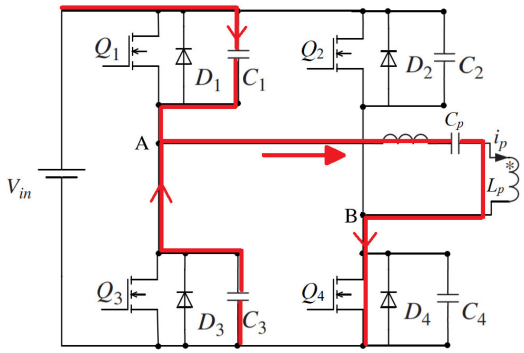

(b) $[t_1, t_2]$

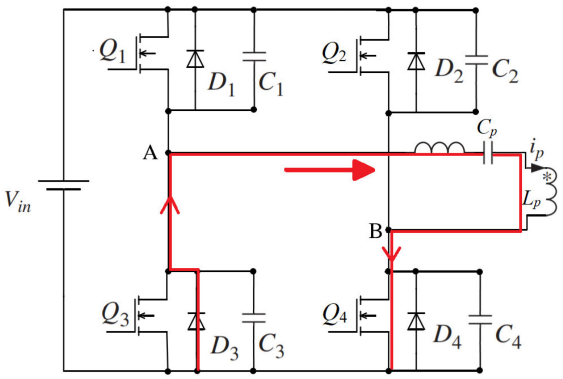

(c) $[t_1, t_2]$ when the voltage of Q_3=0

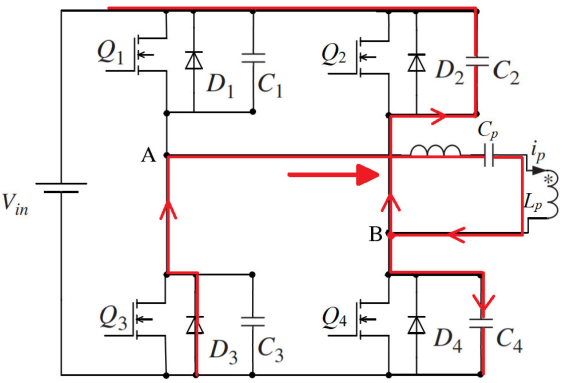

(d) $[t_2, t_3]$

Figure 9. *Cont.*

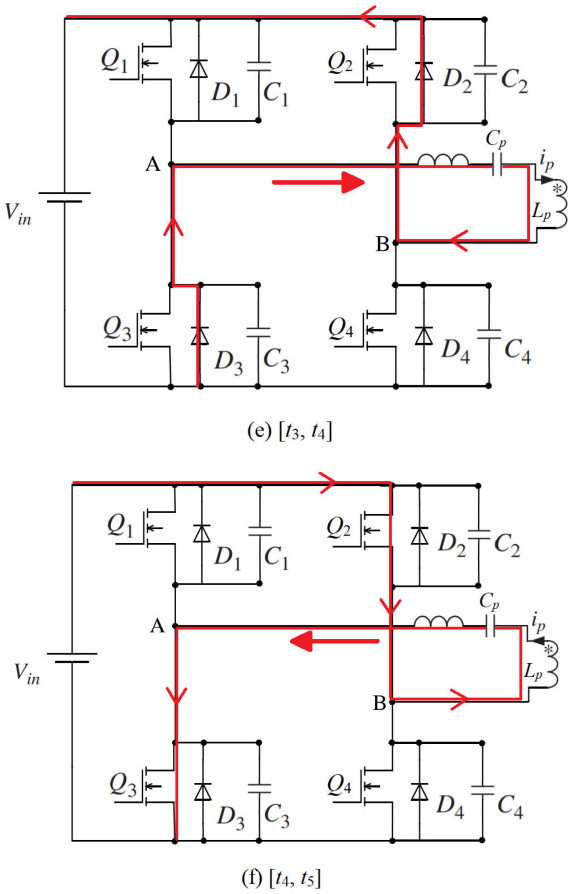

Figure 9. Equivalent circuits of different switching modes in soft-switching condition.

1. Mode 0 [t_0, t_1] (Figure 9a):

   Both Q_1 and Q_4 are on. $U_{AB} = V_{in}$. The primary current i_p goes from point A to point B.

2. Mode 1 [t_1, t_2] (Figure 9b,c):

   At t_1, Q_1 is turned off. The primary current i_p begins to charge C_1 and discharge C_3, as shown in Figure 9b. The voltage of the two capacitances gradually changes. When the voltage of C_1 increases to V_{in} and the voltage of C_3 decreases to 0, this makes D_3 conduct, clamping the voltage of C_3 at 0, as shown in Figure 9c. Therefore, if Q_3 turns on after that time, it can achieve ZVS.

3. Mode 2 [t_2, t_3] (Figure 9d):

   At t_2, Q_4 is turned off. The primary current i_p charges C_4 and discharges C_2. Since the primary side of the circuit is now inductive, the time for the current to drop to 0 can be greatly increased, providing additional time for the charging and discharging process. As a result, C_2 can successfully end the discharge process until D_2 turns on and clamps the voltage of Q_2 to 0, as shown in Figure 10. This provides a prerequisite for Q_2 to realize ZVS conduction.

4. Mode 4 [t_3, t_4] (Figure 9e):

   The charging and discharging process is completed at t_3. If Q_2 turns on after t_3, it can achieve ZVS. After t_3, Q_2 and Q_3 have already turned on. $U_{AB} = -V_{in}$. i_p goes down linearly to 0 and then begins to increase reversely.

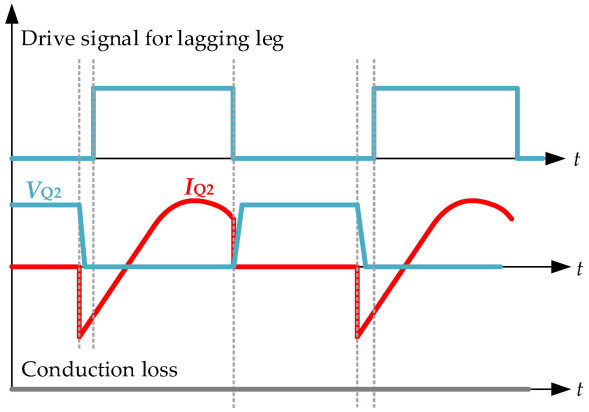

Figure 10. Key waveforms of Q_2 under ZVS conduction.

5. Mode 5 [t_4, t_5] (Figure 9f):

i_p still increases during this period. At t_6, Q_3 is turned off and the circuit operates similarly to Mode 1, which is the beginning of the second switching period. The second half-switching period is similar to the first half period.

As can be seen from Figure 9, the auxiliary inductance can solve the hard-switching problem of the lagging leg. After adding the auxiliary inductance, the current and voltage overlapping area disappear, resulting in almost no conduction loss. Hence, the efficiency is improved compared to the previous one. Moreover, the added inductance does not affect the work of the control loop, so the improved WPT system can realize soft-switching conduction while controlling the output voltage.

In order to simplify the circuit and reduce the EMI brought by the auxiliary inductance, it can be considered making the primary side circuit inductive without auxiliary inductance. Since the operating frequency of the resonant tank is inconvenient to adjust, the resonant capacitance on the primary side can be changed. Increasing the capacitance value can make the primary side circuit inductive rather than resistive at the original resonant frequency. The resonator on the secondary side still works as a fully compensated mode at the initial operating frequency, so it remains resistive. This improvement method just replaces the auxiliary inductance by adjusting the circuit parameters to make the circuit inductive. It does not affect the control circuit.

4. Simulation Results

Three simulations were performed as follows:

1. First, the experiment observes whether the control circuit can stabilize the system output voltage at the reference value. At the same time, the current and voltage waveform of the lagging leg in the circuit is observed to determine whether ZVS can be achieved.

2. Then, according to the increase in the auxiliary inductance, the switch tubes can all work in the conduction state of the soft switch so that the loss of the circuit can be significantly reduced.

3. Finally, when the power supply voltage fluctuates, and the load resistance fluctuates, the system can still output an ideal voltage to ensure the soft-switching working state.

The parameter values of the switch tube are unchanged in the three simulations and they are shown in Table 2.

Table 2. MOSFET Ratings.

Name	Value
Conducting resistance R_{ds} (ON)	0.075 Ω
Diode threshold voltage	200 V
Diode resistance	0.01 Ω
MOSFET parallel capacitance C_{oss}	315 pF

4.1. Simulation of WPT Systems without Auxiliary Circuits

The circuit does not contain the auxiliary inductance and the resonator operates at the resonant frequency. The full-bridge inverter works in the phase shift mode, and the four switches are controlled by the PS modulation. Tables 3 and 4 show the values of various parameters in the circuit. In Table 4, K_P and K_I are the parameters of the PI controller. K_P represents the proportional control coefficient, and K_I represents the integral control coefficient.

Table 3. Key ratings in main circuit.

Name	Value
Input voltage (V_{in})	380 V
Reference output voltage (V_0)	48 V
Primary side resonant capacitance (C_p)	42 nF
Secondary side resonant capacitance (C_s)	41.6 nF
Primary side resonant inductance (L_p)	60.9 μH
Secondary side resonant inductance (L_s)	60.8 μH
Mutual inductance (L_m)	12.17 μH
Primary leakage resistance (R_p)	0.15 Ω
Secondary leakage resistance (R_s)	0.15 Ω
Coupling coefficient K	0.2
Load resistor R_0 (light load condition)	120 Ω
Switching frequency	100 kHz
Filter capacitance (C_f)	100 pF
Filter capacitance resistance (R_f)	0.005 Ω

Table 4. Key ratings in control circuit.

Name	Value
K_P	0.5
K_I	50
Reference voltage (V_{ref})	48 V

Under light load conditions, the phase of the control circuit output reaches more than 160°. As shown in Figure 11, the output phase reaches 178.6°. When the circuit reaches a stable state, the output voltage is consistent at 48.13 V, which is very similar to the reference voltage.

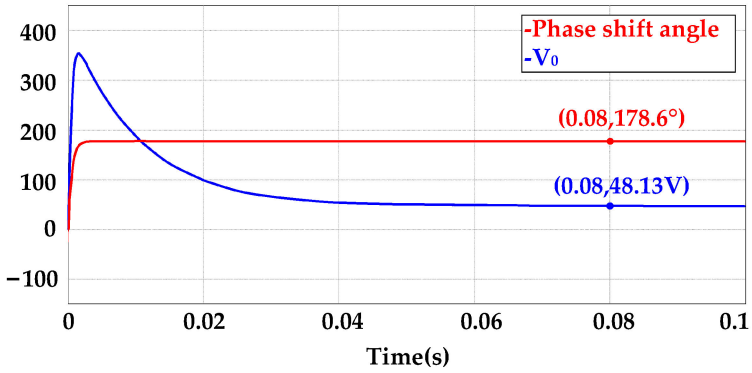

Figure 11. The waveform of output voltage and the phase shift angle in WPT system without optimization.

The voltage and current waveforms when the leading leg Q_1 is turned on and off are shown in Figure 12. It can be seen that when Q_1 is turned on, there is no overlap area between the voltage and current, indicating that Q_1 can realize ZVS conduction and Q_1 has no conduction loss. The voltage and current waveform of Q_3 is exactly the same as that of Q_1, so there is no hard-switching problem in the leading leg in the WPT system. The upper

part of Figure 12 is an overview of the waveforms, and the lower part shows the details of the voltage and current waveforms when Q_1 conducts.

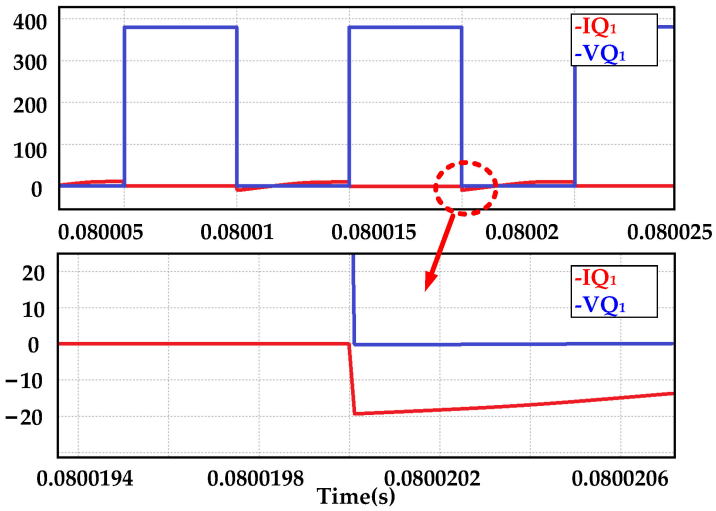

Figure 12. Current waveform and voltage waveform of Q_1 in WPT system without optimization.

Figure 13 shows the voltage and current relationship of Q_2 during operation. It can be seen that when Q_2 is turned on, the current increases, while the voltage decreases, and the two have an overlapping area. The part covered by the dotted line in the black circle in Figure 13 is the conduction loss generated by Q_2. Q_4 works the same as Q_2. The lagging leg cannot achieve soft switching when turning on, resulting in conduction loss. These losses reduce the overall efficiency of the circuit.

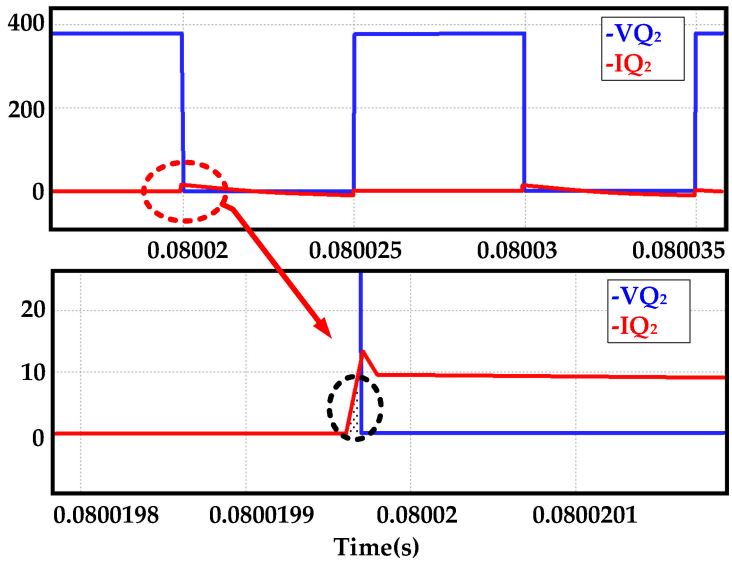

Figure 13. Current waveform and voltage waveform of Q_2 in WPT system without optimization.

According to the simulation results, it can be concluded that the control circuit in the WPT system can make the circuit output an ideal voltage. However, in the full-bridge converter, there is conduction loss in the lagging leg, so the efficiency of the circuit decreases.

4.2. Simulation of WPT Systems with Auxiliary Circuits

According to the theory in Section 3, an inductance is added to the resonant tank in this simulation. The inductance is 20 μH, and the rest of the circuit remains the same. The simulation verifies whether the conduction loss can be reduced, while the output voltage is still controllable under the original circuit parameters. Therefore the circuit is the same as

the first simulation except that inductance is added. The structure and parameters of the control circuit are also completely unchanged.

Figure 14 shows the output voltage when the system is stable and the phase difference. The simulation time is set to 0.15 s. It can be seen that the system output voltage can quickly reach 48.2 V within 0.15 s. When the system reaches the steady state, the phase difference between the leading leg and the lagging leg is different. However, both can output the ideal voltage in time so that the control circuit can work well in the improved system.

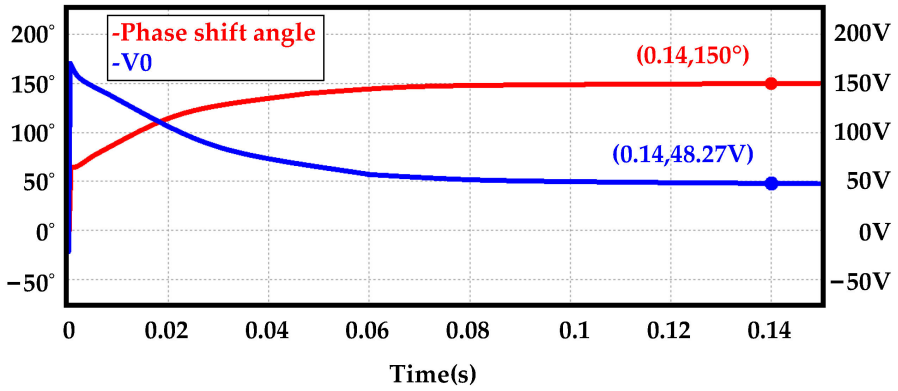

Figure 14. The waveform of output voltage and the phase shift angle in the optimized circuit.

Figure 15 shows the current–voltage waveforms of Q_1 at the turning on stage. Q_1 can still achieve soft switching. The voltage and current waveforms of Q_3 are the same as those of Q_1. The added auxiliary inductance does not affect the working state of the leading leg.

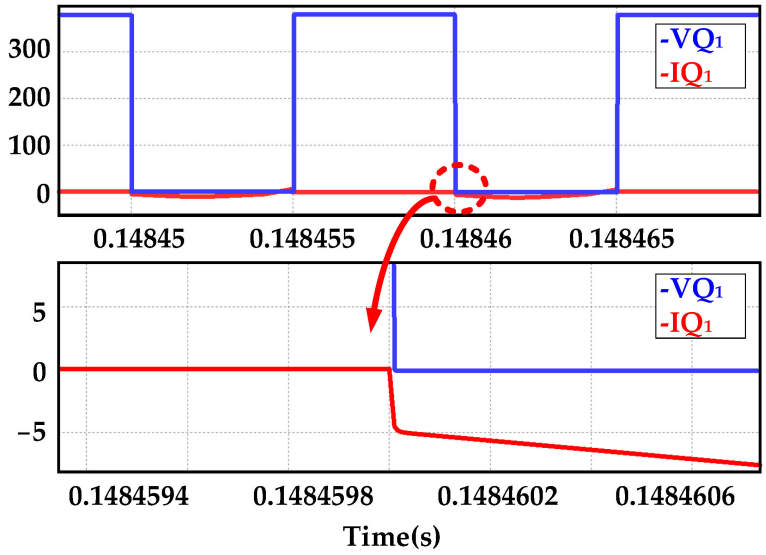

Figure 15. Current waveform and voltage waveform of Q_1 in the optimized circuit.

Figure 16 shows the current and voltage waveforms when Q_2 is turned on. In the black circle, the current and voltage have no overlapping area. The current of Q_2 shows the same trend as Q_1. It increases in the negative direction and then rises again. This is because the discharge current does not decrease to 0 before Q_2 turns on. The current direction is opposite to Q_2's voltage direction, which means that Q_2 has completed the discharge process before turning on. Therefore, ZVS can be turned on. The conduction process of Q_4 is the same as that of Q_2. The lagging leg can achieve ZVS conduction with the help of the auxiliary inductance.

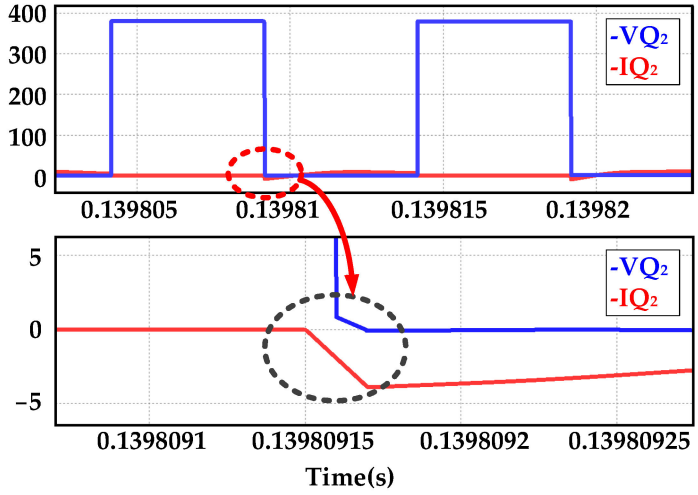

Figure 16. Current waveform and voltage waveform of Q_2 in the optimized circuit.

4.3. Simulation of WPT System with Auxiliary Inductance in Special Cases

In order to verify the stability of the system, the input of the DC power supply is fluctuated by ±10% and the load resistance is adjusted at another moment. In the simulation, the load resistance is set to abruptly change at 0.1 s. The power supply voltage is set to have the maximum voltage fluctuation at 0.2 s in this simulation. The circuit parameters of the circuit are completely consistent with the former simulation, and the parameters of the control circuit also remain unchanged.

According to Figure 17, at 0.1 s, the load suddenly changed from 120 Ω to 20 Ω at 0.1 s. The power supply voltage changed from 380 V to 418 V at 0.2 s. The two areas inside the black circle are the fluctuation of the output voltage, but the output voltage recovered to the reference voltage of 48 V quickly. At the moment of 0.2 s, the power supply voltage fluctuated to the greatest extent, and the output voltage was immediately affected, resulting in a slight fluctuation. However, the voltage also recovered to 48.2 V within 0.5 s and then slowly returned to the exact 48 V.

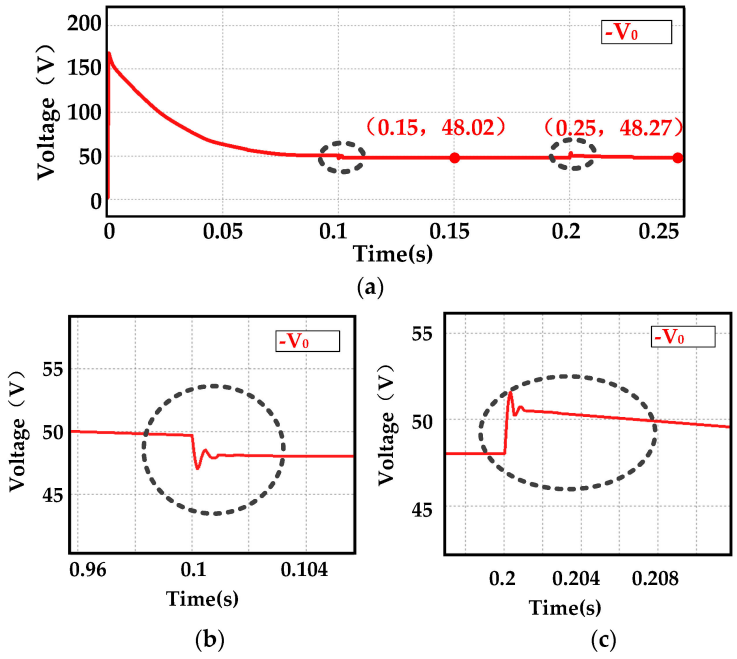

Figure 17. The waveform of output voltage. (**a**) is the overview waveform; (**b**) is the detail waveform when the resistor changes; (**c**) is the detail waveform when the input voltage changes.

Figure 18a shows the waveform of the voltage and current of the lagging leg when the load changes. Figure 18b shows the waveform of the lagging leg when the input voltage changes. Both of the two waveforms are obtained when the system becomes stable again. After changes, the voltage can always return to the referenced value and there were still no hard-switching issues in the circuit.

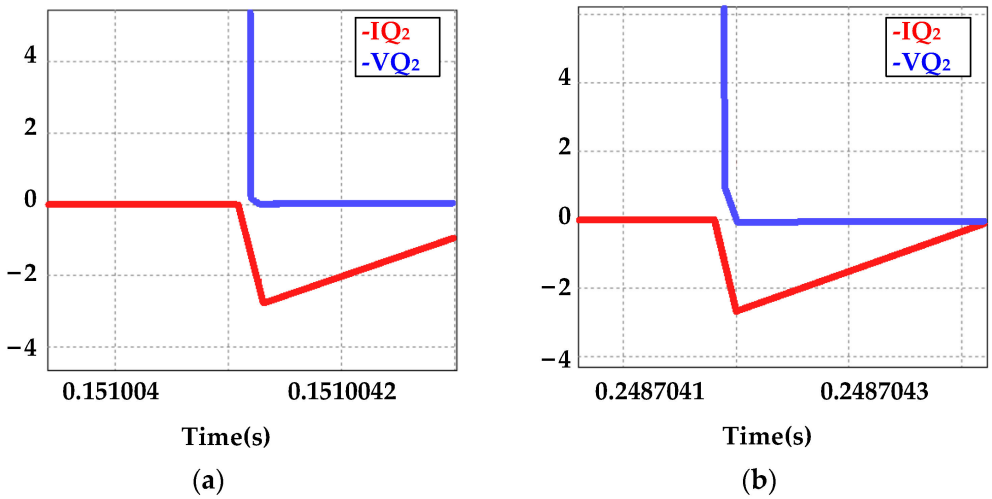

Figure 18. (**a**,**b**) are the waveform diagrams of the current and voltage of Q2 when the output voltage is stable, respectively.

5. Experimental Verification

5.1. Experimental Setup

In order to verify whether the auxiliary inductance can achieve ZVS, experiments were conducted without auxiliary inductance first. Then an auxiliary inductor was added at the primary side circuit for comparison. Both experiments should satisfy that the output voltage is controllable. The current and voltage waveforms of output on the full-bridge inverter side and input on the full-bridge rectifier side are observed with an oscilloscope. The full-bridge inverter adopts the phase shift control mode. The topology of the experimental setup is shown in Figure 19. As shown in Figure 19, the circuit consists of a DC source, a full-bridge inverter, a resonator, a full-bridge rectifier, and a load

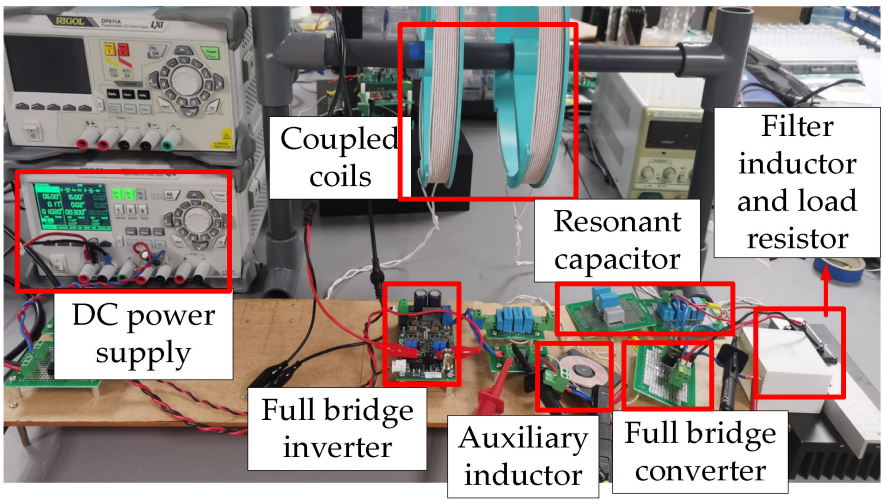

Figure 19. Photograph of the experimental setup.

A scale-down setup is used in the experiment. The experimental parameters are shown in the Table 5.

Table 5. Ratings in experimental circuit.

Name	Value
Input voltage (V_{in})	6 V
Reference output voltage (V_0)	500 mV
Primary side resonant capacitance (C_p)	42 nF
Secondary side resonant capacitance (C_s)	41.6 nF
Primary side resonant inductance (L_p)	60.9 µH
Secondary side resonant inductance (L_s)	60.8 µH
Mutual inductance (L_m)	12.17 µH
Primary leakage resistance (R_p)	0.15 Ω
Secondary leakage resistance (R_s)	0.15 Ω
Coupling coefficient K	0.2
Load resistance (R_0)	5 Ω/10 Ω/15 Ω
Switch frequency	100 kHz
Filter capacitance (C_f)	100 pF
Filter capacitance resistance (R_f)	0.005 Ω
Auxiliary inductance (L_a)	20 µH

5.2. Experiment Results

5.2.1. Experiment of MOSFETs to Realize Soft Switching

Figure 20 shows the system input and output voltage and current waveforms when the load is 10 and 15 without auxiliary circuits. u_{AB} and i_{AB} are the current and voltage of the input side of the resonator, respectively. u_{sed} and i_{sed} are the current and voltage of the output side of the resonator, respectively.

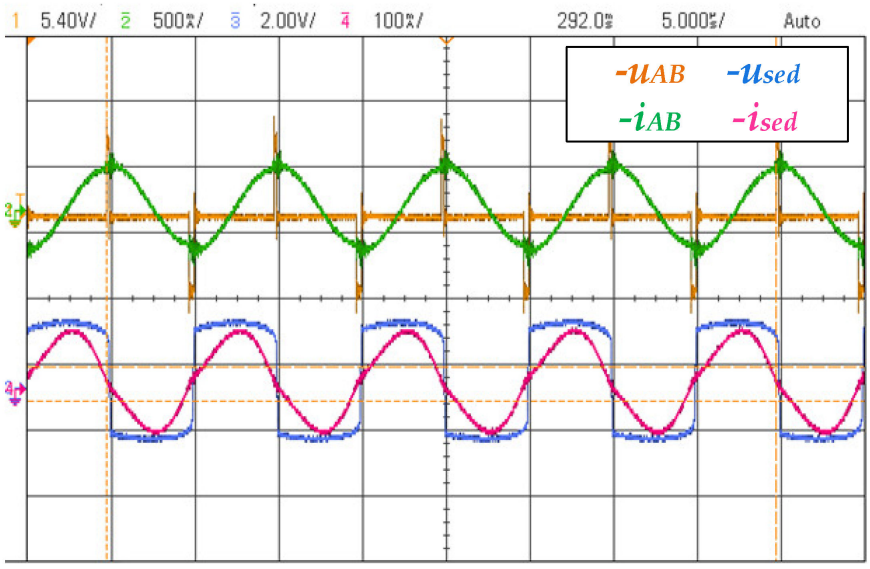

Figure 20. Waveforms of the current and voltage on the primary and secondary sides of the resonator without using auxiliary inductance.

It can be seen from the waveforms of the voltage and the current that the primary side of the circuit is resistive because the resonator was working in a fully compensated state. When the output voltage reaches the reference value of 500 mV, the phase difference is 171°. It can be speculated that the switch tube cannot achieve ZVS. The voltage waveform of the output terminal of the resonator is similar to a rectangular wave. Unlike the voltage waveform of the input side, the waveforms on the output side do not have a large dead zone. The current waveform resembles a sinusoidal waveform. Figure 21 shows the waveforms after adding the auxiliary inductance.

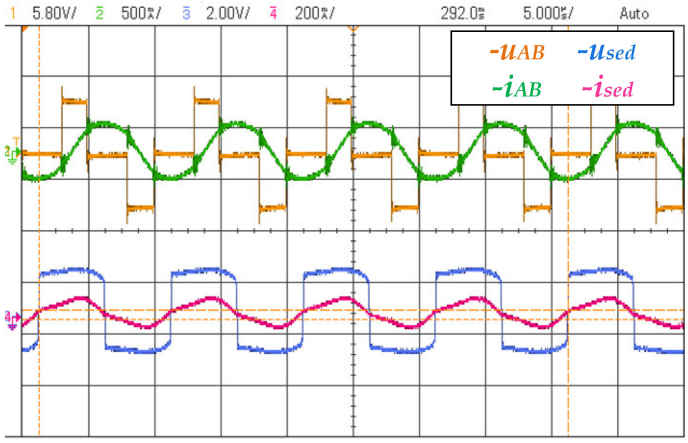

Figure 21. Waveforms of the current and voltage on the primary and secondary sides of the resonator when using auxiliary inductance.

Figure 21 shows that the primary-side output voltage waveform leads the current waveform significantly, indicating that the primary-side loop is inductive. Crucially, it can be seen that when the primary side voltage is reversed, the current has not yet crossed 0 and changed. According to the theory in Section 3, due to the charging and discharging process of the lagging leg, the primary side current does not reverse immediately after the voltage becomes reversed, as shown in Figure 9e. It linearly decreases to 0 and then reverses. Therefore, it can be concluded that the switch tube of the circuit works in a soft-switching state at this time. The conduction losses of the circuit are significantly reduced.

According to the experimental data measured in the experiments, it can be seen that the efficiency of the circuit is improved after using the auxiliary inductance. Figure 22 is a graph derived from all the data. Adding auxiliary circuits can improve the working efficiency of the converter under the majority of load conditions. In particular, when the load is large, the circuit efficiency improvement is more prominent. Moreover, the overall efficiency of the entire WPT system with and without the auxiliary circuit are compared, as shown in Figure 23. Apparently, the overall efficiencies of the system are significantly enhanced by incorporating the auxiliary inductor for lighter load conditions. For heavy load conditions, the difference is not obvious. The main reason is that the phase shift angle of the primary-side inverter is small, such that the switching loss is close to the conduction loss on the auxiliary inductor. Nevertheless, the average efficiency improvement for different load conditions is still considerable, which is about 3%.

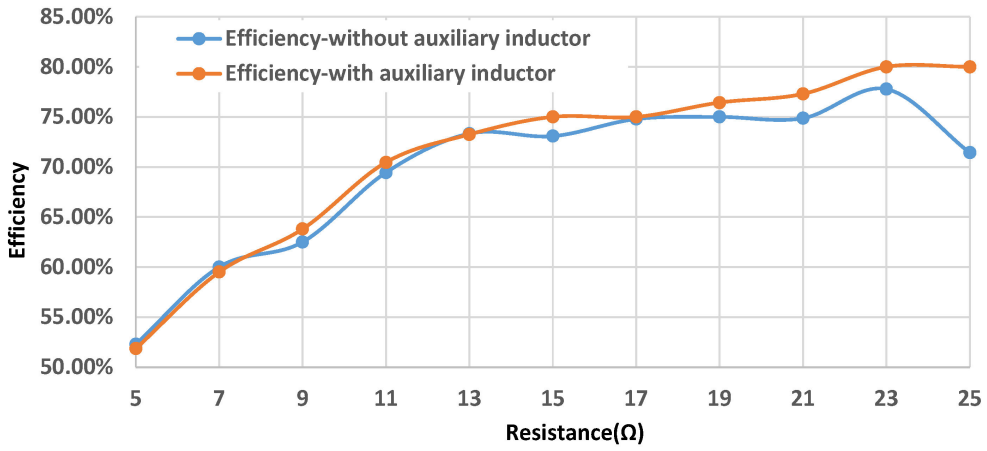

Figure 22. The comparison of the inverter efficiency by adding the auxiliary inductor and without using the auxiliary inductor.

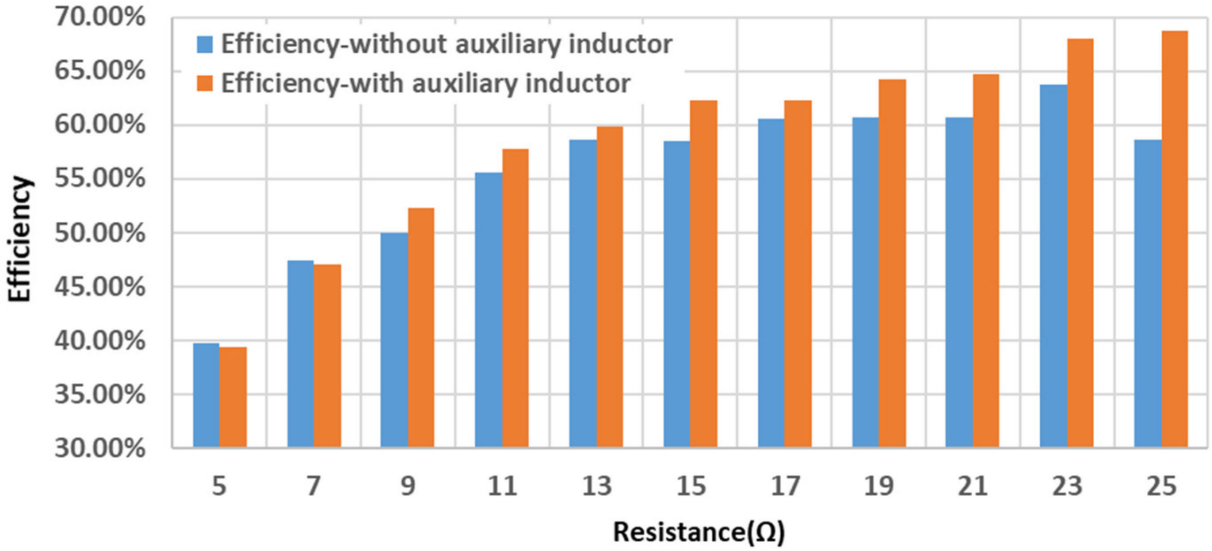

Figure 23. The comparison of the overall system efficiency with and without the auxiliary inductor.

5.2.2. Experiment to Achieve ZVS with the Maximum Power Factor (PF) of the Circuit

The experiment aims to test the optimal resistance value range of the load when adding different auxiliary inductances. Adding an extra series inductor or decreasing the value of the capacitor on the transmitter side resonator can make the system inductive to help the MOSFETs to achieve soft switching. However, when the auxiliary circuit makes the primary circuit more inductive, it also causes more reactive power and reduces the overall efficiency of the circuit. Therefore, it is necessary to discuss the load range corresponding to different degrees of inductive auxiliary circuits so that the circuit can work at high efficiency. When the MOSFETs in the primary side of the circuit can realize ZVS, and PF of the circuit is also the largest, the reactive power in the circuit is the least.

During the charging process of an electric vehicle, the resistance of the battery changes over time. Furthermore, when the electric vehicle still moves, the distance between the primary side coil and the secondary side coil is constantly changing, which causes the mutual inductance fluctuations. Therefore, the experiment is carried on to figure out the relationship between the load resistance and mutual inductance range corresponding to different auxiliary circuits. In the experiment, the primary side of the circuit is made to be inductive by increasing the capacitance of the resonator. In this way, it is only necessary to connect a capacitor parallel with the original circuit to achieve adjustment.

The voltage and current waveforms on the primary side displayed by the oscilloscope are used as a reference to determine whether the MOSFET is at the critical point of hard switching and soft switching. If the current is positive when the voltage jumps from 0 to a positive value, the primary side's MOSFETs work at hard switching, referring to the theory in Section 2. The waveform relationship between voltage and current is shown in Figure 24. u_{AB} and i_{AB} are the voltage and current waveforms of the primary side; u_{sed} and i_{sed} are the voltage and current waveforms of the secondary side. If the current is negative when the voltage jumps from 0 to a positive value, the MOSFETs on the primary side are soft switching, and the circuit on the primary side generates redundant reactive power. The relationship between the voltage and current waveforms is shown in Figure 25. When the voltage suddenly changes and the current is 0 simultaneously, the auxiliary circuit makes the MOSFETs achieve soft switching, while the PF of the circuit is the least. The waveform relationship between the voltage and current at this time is shown in Figure 26.

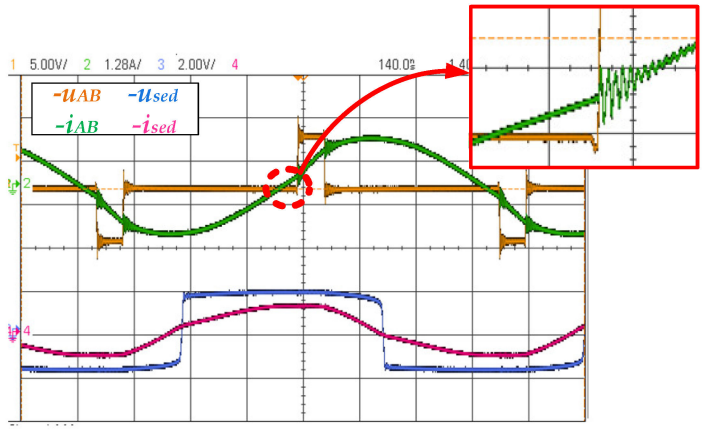

Figure 24. Waveforms of the current and voltage on the primary and secondary sides when the MOSFETs work in hard-switching state.

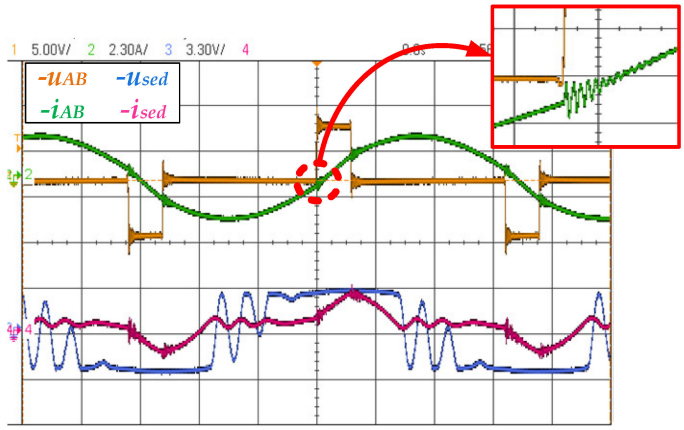

Figure 25. Waveforms of the current and voltage on the primary and secondary sides when the MOSFETs work in soft-switching state with redundant reactive power.

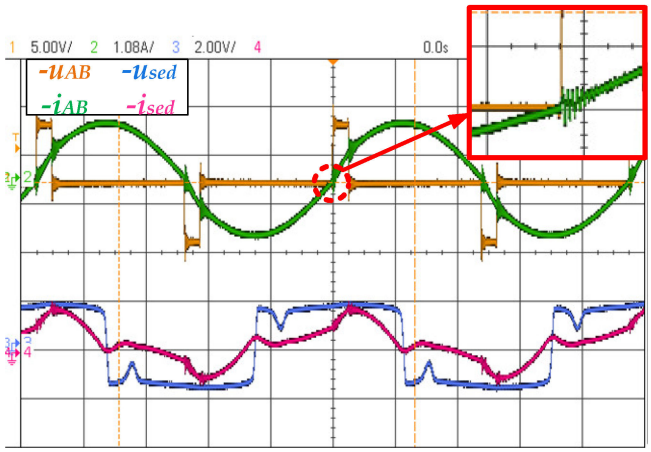

Figure 26. Waveforms of the current and voltage on the primary and secondary sides when the auxiliary circuit can just make the MOSFETs achieve soft switching.

First, the distance of the coil is set to 2.6 cm, and the capacitance value of the auxiliary circuit is adjusted at 5 nF, 9 nF, 11 nF, 13 nF, and 14 nF, respectively. Other parameters of the experiment are shown in the Table 6. After each capacitance is connected in parallel, the load resistance value is adjusted continuously to find when the circuit satisfies soft switching through the oscilloscope. The resistance value is recorded when the MOSFETs

can achieve soft switching with minor reactive power. From the measured data, Figure 27 can be obtained. Under the condition that the distance between the coils remains the same, increasing the capacitance value of the auxiliary circuit increases the upper limit of the circuit load resistance. The recorded resistance value is the maximum load that satisfies the soft-switching condition.

Table 6. Parameters in experimental circuit.

Name	Value
Input voltage (V_{in})	6 V
Reference output voltage (V_0)	500 mV
Primary side resonant capacitance (C_p)	42 nF
Secondary side resonant capacitance (C_s)	41.6 nF
Primary side resonant inductance (L_p)	60.9 µH
Secondary side resonant inductance (L_s)	60.8 µH
Switch frequency	100 kHz
Filter capacitance (C_f)	100 µF

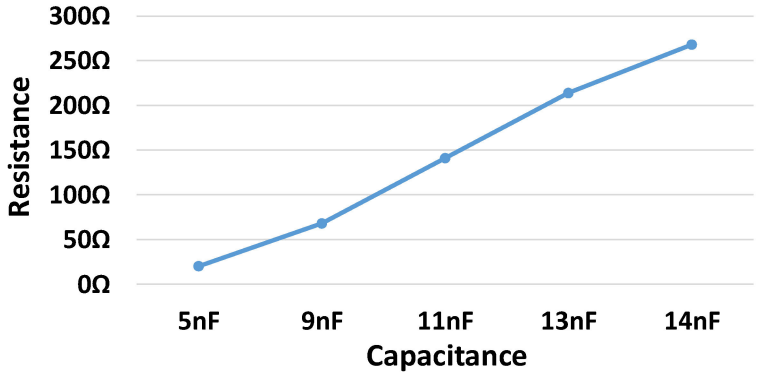

Figure 27. The curve of the maximum value of the load resistance, after five groups of auxiliary capacitors are connected in parallel.

The relationship between the coil distances corresponding to different capacitance values is tested while the load resistance remains unchanged. The load resistance is set to be 40 Ω. The different capacitance values are the same as in the previous experiment. The experiment tested the coil distance to make the MOSFETs achieve soft switching with minor reactive power. Figure 28 is obtained according to the measured data. It can be seen that when the coil distance becomes smaller, a larger capacitance needs to be provided to enable the primary side switch tube to achieve soft switching.

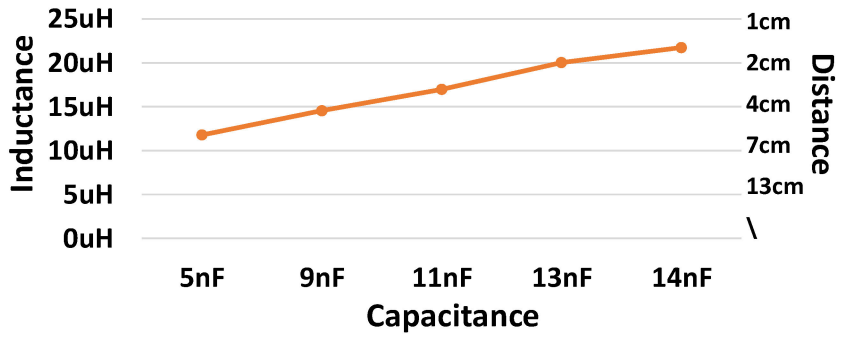

Figure 28. The curve of the distance of the coupled coil, after five groups of auxiliary capacitors are connected in parallel.

During static charging, considering that the resistance of the battery will continue to increase, it is necessary to increase the inductance or capacitance of the auxiliary circuit to

maintain the soft-switching state of the circuit. During dynamic charging, the mutual inductance changes the coil misalignment. Electric vehicles can switch capacitors in different gears according to the changing trend of the auxiliary capacitances tested in the paper to make the circuit achieve ZVS.

6. Conclusions

This paper proposes an auxiliary method to help the switches in the full-bridge inverter achieve soft switching in WPT systems. By adding an auxiliary inductance on the primary side of the resonator, the MOSFETs can easily achieve ZVS, thereby reducing the conduction loss. Both the simulation and experiments confirm that the increased auxiliary inductance can improve the efficiency of the circuit according to less conduction loss without affecting the operation of the control circuit. Meanwhile, the simulation verifies that the control circuit can still work with the auxiliary inductance even when the power grid fluctuates or the load changes. Finally, the paper simulates the requirements for auxiliary circuits when charging electric vehicles in different scenarios through experiments. The empirical results reveal that the auxiliary inductor can significantly improve the efficiency of entire WPT systems with light load conditions, while the improvement is not obvious for heavy load conditions.

Author Contributions: H.X. was responsible for the writing of the methodology, simulation verification, and experiments in the paper. The supervision, review and editing of the papers were mainly carried out by B.X. and Y.M. All authors have read and agreed to the published version of the manuscript.

Funding: This research received no external funding.

Conflicts of Interest: The authors declare no conflict of interest.

References

1. Rim, C.T.; Chris, M. *Wireless Power Transfer for Electric Vehicles and Mobile Devices*; Wiley: New York, NY, USA, 2017.
2. Covic, G.A.; Boys, J.T. Inductive power transfer. *Proc. IEEE* **2013**, *101*, 1276–1289. [CrossRef]
3. Dragičević, T.; Lu, X.; Vasquez, J.C.; Guerrero, J.M. DC Microgrids—Part II: A Review of Power Architectures, Applications, and Standardization Issues. *IEEE Trans. Power Electron.* **2016**, *31*, 3528–3549. [CrossRef]
4. Yang, Y.; Tan, S.C.; Hui, S.Y.R. Mitigating distribution power loss of DC microgrids with DC electric springs. *IEEE Trans. Smart Grid* **2017**, *9*, 5897–5906. [CrossRef]
5. Yang, Y.; Qin, Y.; Tan, S.C.; Hui, S.Y.R. Efficient improvement of photovoltaic-battery systems in standalone DC microgrids using a local hierarchical control for the battery system. *IEEE Trans. Power Electron.* **2019**, *34*, 10796–10807. [CrossRef]
6. Deng, J.; Mao, Y.; Yang, Y. Distribution power loss reduction of standalone DC microgrids using adaptive differential evolution-based control for distributed battery systems. *Energies* **2020**, *13*, 2129. [CrossRef]
7. Qian, X.; Yang, Y.; Li, C.; Tan, S.C. Operating cost reduction of DC microgrids under real-time pricing using adaptive differential evolution algorithm. *IEEE Access* **2020**, *8*, 169247–169258. [CrossRef]
8. Yang, Y.; Tan, S.C.; Hui, S.Y.R. State-of-charge balance control of distributed battery systems with distinct state-of-health in DC microgrids. In Proceedings of the IEEE/IAS Industrial and Commercial Power System Asia (I & CPS Asia), Chengdu, China, 18–21 July 2021; pp. 140–144.
9. Yang, Y.; Zhong, W.; Kiratipongvoot, S.; Tan, S.C.; Hui, S.Y.R. Dynamic improvement of series-series compensated wireless power transfer systems using discrete sliding mode control IEEE Trans. *Power Electron.* **2017**, *33*, 6351–6360. [CrossRef]
10. Yang, Y.; Tan, S.C.; Hui, S.Y.R. Communication-free control scheme for Qi-compliant wireless power transfer systems. In Proceedings of the IEEE Energy Conversion Congress and Exposition (ECCE), Baltimore, MD, USA, 29 September–3 October 2019; pp. 4955–4960.
11. Yang, Y. Development of front-end monitoring of mutual coupling and load conditions in wireless power transfer systems. In Proceedings of the 8th International Conference on Power Electronics Systems and Applications (PESA), Hong Kong, China, 7–10 December 2020; pp. 1–5.
12. Li, S.Y. Design of 75kW Phase-Shifted Full-Bridge ZVS DC/DC Converter. Master's Thesis, Harbin Institute of Technology, Harbin, China, June 2015.
13. Deng, J.J. Research on High-Efficiency Resonant Converter of On-Board Charger for Electric Vehicle. Ph.D. Thesis, Northwestern Polytechnical University, Xi'an, China, November 2015.
14. Roslan, M.A.A.; Nanda, N.N.; Yusoff, S.H. Series-series and series-parallel compensation topologies for dynamic wireless charging. *Iiumej* **2021**, *22*, 199–209. [CrossRef]

15. Tang, X.C. Research on LLC Resonant Converter Based on Digital Control. Master's Thesis, Nanjing University, Nanjing China, March 2012.
16. Wan, C.A.; Liu, W.G. Active Clamp ZVS-PWM Switching Converter Application. *Aerosp. Technol.* **2000**, *1*, 21–25.
17. Cos Mart, O. Digital Control Strategy for LLC Converter. Master's Thesis, Universitat Politecnica de Catalunya, Barcelona, Spain, October 2020.
18. Zhou, K.; Liu, Y.; Wu, X. Research on Wide Input Voltage LLC Resonant Converter and Compound Control Strategies. *Electronics* **2022**, *11*, 3379. [CrossRef]
19. Lee, F.C. High-frequency quasi-resonant converter technologies. *Proc. IEEE* **1988**, *76*, 377–390. [CrossRef]
20. Tabisz, W.A.; Lee, F.C. DC analysis and design of zero-voltage-switched multi-resonant converters. In Proceedings of the 20th Annual IEEE Power Electronics Specialists Conference, Milwaukee, WI, USA, 26–29 June 1989; Volume 1, pp. 243–251.
21. Ruan, X.B. *Soft-Switching Technology of DC Switching Power Supply*, 2nd ed.; Science Press: Beijing, China, 2003; pp. 118–134.
22. Narimani, M.; Moschopoulos, G. A new DC/DC converter with wide-range ZVS and reduced circulating current. *IEEE Trans. Power Electron.* **2013**, *28*, 1265–1273. [CrossRef]
23. Yadav, G.N.B.; Narasamma, N.L. An active soft switched phase-shifted full-bridge DC-DC converter: Analysis, modeling, design, and implementation. *IEEE Trans. Power Electron.* **2014**, *29*, 4538–4550. [CrossRef]
24. Safaee, A.; Jain, P.K.; Bakhshai, A. An adaptive ZVS full-bridge DC-DC converter with reduced conduction losses and frequency variation range. *IEEE Trans. Power Electron.* **2015**, *30*, 4107–4118. [CrossRef]
25. Chen, Z.; Wang, Y.; Li, M.N. Wide range zero voltage switching phase-shifted full-bridge converter with low circulation loss. *Trans. China Electrotech. Soc.* **2015**, *30*, 71–79.
26. Chen, Z.; Liu, S.; Wang, Y. A new ZVS full-bridge converter with active-regulating auxiliary current. *Trans. China Electrotech. Soc.* **2014**, *29*, 1–9.
27. Sun, T.C.; Guo, C.; Naren, T. A novel DC-DC ZVS full-bridge converter based on phaseshift control. *Trans. China Electrotech. Soc.* **2014**, *29*, 66–72.
28. Li, H.M.; Zhang, H.G.; Cui, C. A review of research on PWM soft-switching DC-DC converters for on-board charging. *Trans. China Electrotech. Soc.* **2017**, *32*, 59–70.